Magnetic Compton scattering study of the Co_2FeGa Heusler alloy: Experiment and theory

Aniruddha Deb,* M. Itou, and Y. Sakurai
Japan Synchrotron Radiation Research Institute (JASRI), SPring-8, 1-1-1 Kouto, Mikazuki, Sayo, Hyogo 679-5198, Japan

N. Hiraoka and N. Sakai
Department of Material Science, Himeji Institute of Technology, 1-2-3, Kamigori, Ako, Hyogo 678-1297, Japan
(Received 10 July 2000; published 19 January 2001)

The spin density in Co_2FeGa Heusler alloy has been measured in a magnetic Compton scattering experiment using 274-keV circularly polarized synchrotron radiation at the high energy inelastic scattering beamline (BL08W) at SPring-8, Japan. A detailed band-structure calculation including hyperfine field study was performed utilizing the generalized gradient corrected full-potential linear augmented plane-wave (FLAPW-GGA) method. The magnetic Compton profiles for the [100], [110], and [111] principal directions, reported here, show anisotropy in the momentum density which is in good agreement with the FLAPW-GGA results based on ferromagnetic ground state. The conduction electrons were found to have a negative spin polarization of $0.60\mu_B$, which is at variance with the prediction of a positive moment from the recent neutron data. In the calculation, $3d$ spin moment at the Co and Fe site was found to be $1.20\mu_B$ and $2.66\mu_B$, and their respective contribution in the e_g and t_{2g} sub-bands are in excellent agreement with the earlier reported neutron-diffraction measurements. It is also seen from our calculated results that the Co and Fe moment are mainly e_g in character.

DOI: 10.1103/PhysRevB.63.064409 PACS number(s): 75.25.+z, 78.70.Ck, 71.15.Ap, 75.20.Hr

I. INTRODUCTION

Heusler alloys are ternary intermetallic compounds with stoichiometric composition X_2YZ, where X can be a $3d$, $4d$, or $5d$ element (e.g., Co, Fe, Ni, Cu, . . .); Y can be Ti, V, Cr, Mn, Fe and Z is, for example, Al, Si, Ga, As, In, or Sn. Heusler alloys are interesting magnetic systems because they possess localized magnetic moments, although they are all metallic. Heusler alloys have a $L2_1$ lattice structure, where each X atom has four Y atoms and four Z atoms as the nearest neighbors and each Y or Z atom is surrounded by eight X atoms. If X and Y are magnetic, they influence each other's magnetic properties. The formation and coupling of the magnetic moment in Heusler alloys are still the subject of numerous theoretical and experimental studies. The Mn atom at the Y site in X_2MnZ carries a large magnetic moment $(3-4\mu_B)$, while Mn at an X site in Mn_2VAl carries a small amount $(1-2\mu_B)$.[1] Many Co Heusler alloys with chemical formula Co_2YZ have been discovered and it was found that the Co atom carries a small magnetic moment (less than $1\mu_B$). Webster[2] observed that the Co and the Mn moments in Co_2MnZ are larger for the alloys containing the IVb elements (Z=Si, Ge, and Sn) than for the alloys containing IIIb elements (Z=Al and Ga). Hyperfine fields at Co and Mn sites in Co_2MnZ (Z=Si, Ge, Sn, Al, and Ga) have been observed.[3–6] The Mn hyperfine field was found to be roughly proportional to the Mn moment, while Co hyperfine field was not proportional to the Co moment. Furthermore, the experimental results show that the Co hyperfine field in Co_2YZ changes drastically with increasing number of valence electrons of the Y atom (Y=Ti, V, Cr, Mn, Fe).

The formation and coupling of the magnetic moments in Mn related Heusler alloys have been studied widely theoretically and experimentally. From the early neutron-scattering experiments performed on Cu_2MnAl, Pd_2MnSn, and Ni_2MnSn samples[7–9] it was concluded that the $3d$ electrons are well localized on the Mn atoms and in the Heusler alloys the interactions are long range, extending to more than eight neighbors. These Mn-Mn large distance interactions are interpreted by an s-d interaction of the Ruderman-Kittel-Kasuya-Yosida type.

A number of theoretical calculations of electronic structure and magnetic-moment formation in Heusler alloys,[10–14] accompanied the earlier experimental reports. Ishida *et al.*,[14] performing band-structure calculations for Co_2MnSn, Co_2TiSn, and Co_2TiAl, showed that the small humps of the density of states near the Fermi level determined the small Co magnetic moment of Co_2YZ. The Korringa-Kohn-Rostoker calculations of electronic and magnetic properties of Co_2MnZ (Z=Ai, Ga, Si, Ge, and Sn) by Fujii *et al.*[13] showed that the magnetic moments and the hyperfine fields on the Co and Mn are influenced by the nonmagnetic Z atom. A similar approach to Co-Ni Heusler alloys, with detailed band-structure calculations, has been presented by Tobola *et al.*[15]

Though many theoretical and experimental studies on the electronic structure of Heusler alloys of the form X_2YZ where Y=Mn have been reported earlier, the compound in question here (Co_2FeGa) has been earlier studied by Buschow *et al.*[16] and very recently by Brown *et al.*[17] utilizing polarized neutron-diffraction measurement. In their neutron diffraction study Brown *et al.*[17] obtained a small positive delocalized moment for Co_2FeGa and Co_2MnGe contrary to the other Co-based Heusler alloys where delocalized moment were found to be small and negative. Thus bearing these considerations in mind, it seemed worthwhile to undertake an experimental-theoretical study of Co_2FeGa Heusler alloy, and motivated us for the present experimental Compton scat-

 ©2001 The American Physical Society

tering investigation. With the more direct access to the spin-dependent electron momentum density provided by the magnetic Compton scattering technique, we decided to confront highly accurate full-potential linear augmented plane-wave method utilizing the generalized gradient approximation scheme (FLAPW-GGA) computations with the corresponding measurements. Another reason for interest in this compound is the recent excitement in these alloys triggered by the possibility that they are half metallic ferromagnets. For half metallic ferromagnetic systems, the density of states at the Fermi level for one sub-band is very small whereas that of the other is large. It should be noted that these systems exhibit metallic behavior for electrons of one spin state and insulating for the other. The potential technological importance of half-metallic ferromagnets,[18,19] e.g., spin valves, made this class of compounds to be the subject of ongoing experimental[18] and theoretical[19] studies. Half metallic ferromagnets was reported[20] in intermetallic compounds containing manganese, with semi-Heusler cubic $C1_b$ structure such as NiMnSb. Moreover, recent band-structure calculations have reported identical properties for related iron and cobalt based Heusler alloys,[21] CrO_2,[22,23] and doped manganese perovskites.[24] Half metallic behavior has been predicted for Co_2MnSi,[21] which is a member of the series of ferromagnetic Heusler alloys in which both cobalt and manganese atoms carry moments. It is well established that the magnetic properties of these compounds depend sensitively on the degree of atomic order and on the conduction electron concentration.[25] The purpose of this present calculation is also to obtain evidence for the half metallic behavior.

The outline of this paper is as follows. The introductory remarks are followed by Sec. II which gives the salient features of the FLAPW-GGA computations. Section III is devoted to the relevant details of experiment and data processing. The band structure and the hyperfine fields are presented in Sec. IV. In Sec. V the total and the partial densities of states and electron densities are analyzed. The magnetic Compton profiles and their anisotropies are presented in Sec. VI. Finally, the summary and conclusions are given in Sec. VII.

II. HEUSLER STRUCTURE AND METHOD OF CALCULATION

Co_2FeGa at stoichiometry corresponds to an ideal Heusler ($L2_1$) structure compound, having space group $Fm3m$. This structure type, shown in Fig. 1, is based on an underlying bcc arrangement of atomic sites with lattice constant $a/2$, with Ga atoms at (0,0,0), Fe at $(1/2,1/2,1/2)a$, and Co atoms at $(1/4,1/4,1/4)a$ and $(3/4,3/4,3/4)a$, where $a=5.737$ Å is the lattice constant of the resulting fcc compound.

The FLAPW (Ref. 26) method is among the most accurate band-structure methods currently available. In this method the space is divided into an interstitial region and nonoverlapping muffin-tin (MT) spheres centered at the atomic sites. In the interstitial region, the basis set consists of plane waves. Inside the muffin-tin spheres, the basis set is described by radial solutions of the one-particle Schrödinger equation, at fixed energies, and their energy derivatives times

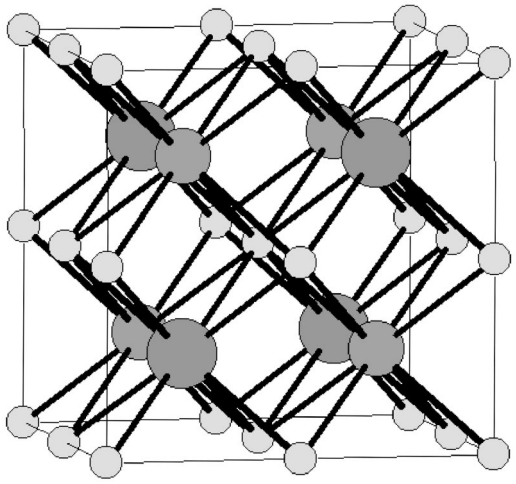

FIG. 1. The crystal structure of the Heusler alloy Co_2FeGa, showing the four interpenetrating fcc sublattices. Co occupy (1/4, 1/4,1/4) and (3/4,3/4,3/4) positions. Fe are at (1/2,1/2,1/2) and Ga at (0,0,0). The medium spheres denote the Fe sites, the small and the large spheres are the Co and Ga sites.

spherical harmonics. Valence states and semicore states (Co $3p$, Fe $3p$, Ga $3d$) were treated in the same energy window by using local orbitals[27] as an extension to the LAPW basis set. This method is based on the first-principles density-functional theory with the generalized gradient approximation (GGA) for the exchange correlation[28,29] throughout. GGA has a stronger formal foundation because it accounts specifically for density gradients that are neglected in local-density approximation (LDA), and does so in a way that satisfies several exact constraints in the form of the exchange-correlation energy functional. It has been seen that GGA seems to give a general improvement in comparison to experimental data for alkali metals,[30] $3d$ and $4d$ transition metals,[31] lanthanides,[32] and ionic insulators.[33] Very recently Deb *et al.*[34] have shown that GGA gives an overall improvement with experimental data for Heusler alloys also compared to LDA. Assessing the differences between GGA and LDA is delicate, requiring in principle a full potential method. The muffin-tin sphere radii R used are 2.2 a.u. for Co and Fe and 2.4 a.u. for Ga. Inside the atomic spheres the charge density and the potential are expanded in crystal harmonics up to $l=6$. The radial basis functions of each LAPW were calculated up to $l=10$ and the nonspherical potential contribution to the Hamiltonian matrix had an upper limit of $l=4$. The Brillouin-zone integration was done with a modified tetrahedron method[35] and we used 227 **k** points in the irreducible wedge of the Brillouin zone (IBZ). The density plane-wave cutoff is $RK_{max}=8.7$, providing well converged basis sets which leads to about 400 basis functions, while the potential cutoff extends up to 14, so no shape approximation to the potential is necessary.

III. EXPERIMENT AND DATA PROCESSING

Compton scattering is an incoherent process, therefore the method can only be applied to the materials with a net magnetic moment, i.e., ferro- or ferrimagnets. Because of the

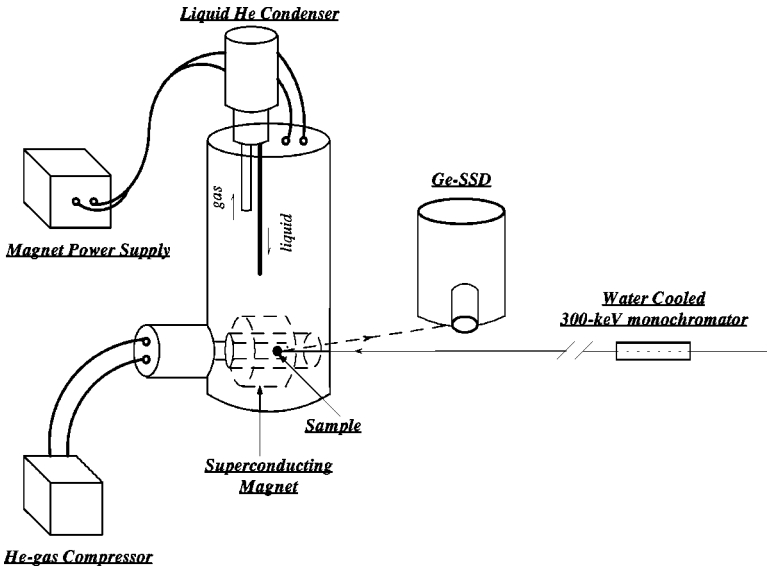

FIG. 2. Schematic of the experimental setup. The scattering geometry using the superconducting magnet. The field is 2.5 T and has a uniformity of 2% over the sample position.

inherently small cross section being involved, magnetic Compton scattering (MCS) experiments have only become feasible with the advent of high-energy synchrotron radiation sources. Measuring alternately the standard Compton profile with opposite sample magnetization, MCS provides information of the momentum distribution of the difference between the spin-up and spin-down electrons. To be sensitive to magnetic electrons, these experiments require circularly polarized photons that couple to the term in the incoherent scattering cross section arising from the interference between charge and magnetic scattering. Comprehensive reviews of Compton scattering related to charge and magnetization densities can be found in Refs. 36–38. Briefly, when linearly polarized radiation is utilized the spectrum of the inelastically scattered radiation can be interpreted, with an impulse approximation, in terms of the projection of the electron momentum distribution, $n(\mathbf{p})$, along the scattering vector. This quantity is referred to as the Compton profile and usually denoted $J(p_z)$ where the z direction is parallel to the scattering vector,

$$J(p_z)=\int\int [n(\mathbf{p})_{\uparrow}+n(\mathbf{p})_{\downarrow}]dp_x dp_y \qquad (1)$$

Here the momentum distribution, $n(\mathbf{p})$, has been split into spin up, $n(\mathbf{p})_{\uparrow}$, and spin down, $n(\mathbf{p})_{\downarrow}$, components. The momentum space wave functions, from which the density distributions are formed, are simply Fourier transforms of their position space counterparts.

When circularly polarized radiation is utilized there is a coupling between charge and spin scattering resulting in a term depending on the spin density. The magnetic Compton profile $J_{mag}(p_z)$, which can be deduced from the scattering cross section, can be expressed as

$$J_{mag}(p_z)=\int\int [n(\mathbf{p})_{\uparrow}-n(\mathbf{p})_{\downarrow}]dp_x dp_y . \qquad (2)$$

Experimentally it can be obtained by the reversal of the direction of the sample magnetization and forming the difference between the spin-up and spin-down signals, thereby eliminating the charge scattering, which is unaffected by the field direction.[39,40] It is important to note that the area under the Compton profile $J(p_z)$, integrated over all momenta, is just equal to the total number of electrons. On the contrary the area under the magnetic Compton profile is numerically equal to the spin moment in Bohr magnetons μ_B.

The Compton measurements on the Co_2FeGa Heusler alloy was performed at the magnetic Compton spectrometer installed at the high energy inelastic scattering beamline BL08W (Station A) at SPring-8, Japan. The x-ray source of this beamline is an elliptic 37-pole wiggler with a critical photon energy of 42.6 keV, where the wiggler was operated with $K_x=0.6$ and $K_y=11.2$. A sketch of the experimental arrangement is shown in Fig. 2. Elliptically polarized 274-keV x rays were monochromatized by an asymmetric Si(771) Johann-type monochromator. The angle of Compton scattering was 175°. The flux at the sample was of the order of 10^{10} photon/s and the degree of circular polarization was about 0.7 with an energy resolution of $\triangle E/E \leqslant 5\times 10^{-3}$. Ingot of Co_2FeGa was examined using the Laue diffraction technique. Single crystals were cut from the ingot in the form of rectangular parallelepipeds with approximate dimensions $8\times 7\times 7$ mm. The samples were mounted in an external field of 2.5 T generated by a superconducting magnet, which is sufficient to saturate the magnetization of the samples at 300 K.

The Compton profiles were measured along the [100], [110], and [111] principal directions. A beam 3 mm high and 1 mm wide was incident on the sample. One interesting feature of this experiment was the use of the superconducting magnet that has been designed and constructed for magnetic Compton profile (MCP) measurements at BL08W. The superconducting magnet is described elsewhere in detail by Sakai *et al.*[41] A maximum magnetic field ± 3 T could be generated with a current of ± 79 A, and the field direction can be altered quickly by changing the current direction (within 5 s), and liquid-He refill is not required for more than a few months, which is long enough to measure an ordinary set of MCP data.

The data were collected using a Ge solid-state detector (Ge SSD). The momentum resolution was 0.66 a.u. (1 a.u. $=1.99\times10^{-24}$ mkg/s), which was mainly restricted by an energy resolution of the Ge SSD. The magnetic field in the sample was reversed in the sequence of $(+,-,-,+,-,+,+,-)$, where $(+)$ and $(-)$ represents the relative direction of the magnetic field [$(+)$ being parallel to the scattering vector and $(-)$ vice versa]. A switching time of 6 s and dwell time of 60 s was used to ensure good signal averaging.

The integrated counts for the momentum range $-10-+10$ a.u. were equal to 7×10^6 under the Compton line in the total (i.e., spin-up plus spin-down) spectrum and 4×10^4 in the spin-dependent Compton profile (i.e., spin-up minus spin-down) for the [110] direction. The measurement time was 32 h. Energy-dependent corrections, namely for absorption in the sample and for the charge and magnetic cross sections, were applied to the raw data. Since the analyzed Compton line lies in a relatively narrow energy range where the efficiency of the Ge SSD is close to 100%, no energy-dependent efficiency correction was deemed necessary. The ordinate of the data has been then transformed from energy to momentum in atomic units and folded about $p_z=0$. Finally the magnetic profiles were normalized to a spin moment per unit formula. The value is deduced to be $5.10\mu_B$ at 300 K from the magnetization data of the Co_2FeGa Heusler alloy by Buschow *et al.*[16]

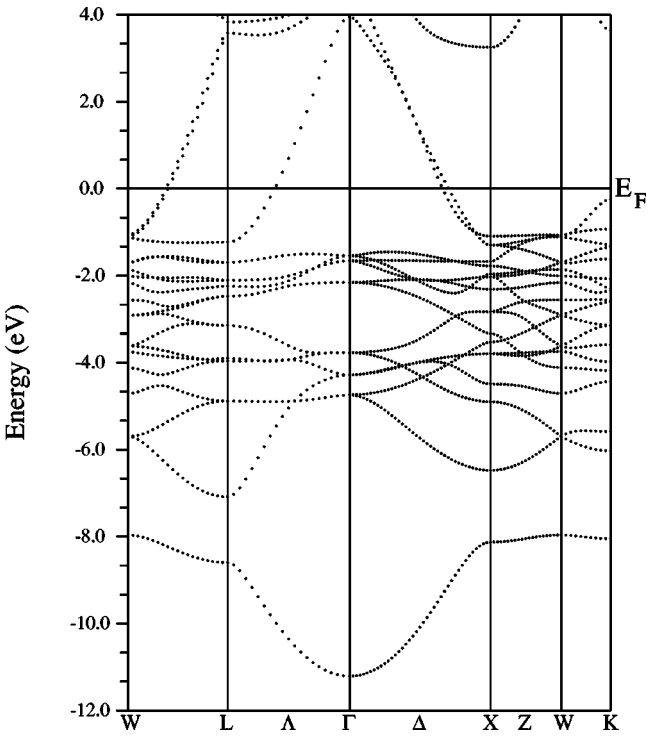

FIG. 3. The FLAPW band structure of ferromagnetic Co_2FeGa along the high symmetry lines for the majority spin.

IV. BAND STRUCTURE AND HYPERFINE FIELDS

The majority and minority (which we will refer to as up and down) band structure resulting from FLAPW-GGA calculation in the high-symmetry directions in the Brillouin zone are shown in Figs. 3 and 4, respectively. The valence band has a band width of 11.2 eV. The lowest valence band, which is separated from the other valence bands by an energy gap of about 0.8 eV for both majority and minority spins, is of Ga 4*s* character along with contributions from Co and Fe 4*s* states. From Fig. 3 it is evident that for the majority spin electrons the band structure has metallic intersections, and band 17 gives rise to a hole pocket centered at Γ. For the minority spin electrons the Fermi level lies just at the bottom of the conduction band (Fig. 4). It is important to note here that an analysis of the eigenvectors allows us to reveal information about the character of the bands. From the character of the bands it is clear that the valence bands are derived from the 3*d* electrons of Co and Fe and Ga 4*s* electrons. The important main results of this analysis are shown in Figs. 5(a)–5(d), where the symbol size used is proportional to the strength of the orbital character of the bands (i.e., the size of each circle is proportional to the partial charge of the specified atom). From the figures it is evident that the lower conduction bands (within 1 eV above the Fermi level) for the minority spin, are made of hybridized bands between Co and Fe *d* orbitals [Figs. 5(b) and 5(d)]. While the majority-spin valence bands (within 6 eV below the Fermi level), are made of hybridized bands between Co and Fe-*d* states [Figs. 5(a) and 5(c)]. It is to be noted that for the minority spin the Co-*d* states extend to 6 eV in the valence band whereas the Fe-*d* states are pronounced in region between 2 and 4 eV in the valence band. Moreover, the Co-3*d* moment and Fe-3*d* moment together with the moments of their e_g and t_{2g} symmetries utilizing the FLAPW-GGA scheme along with available experimental results are

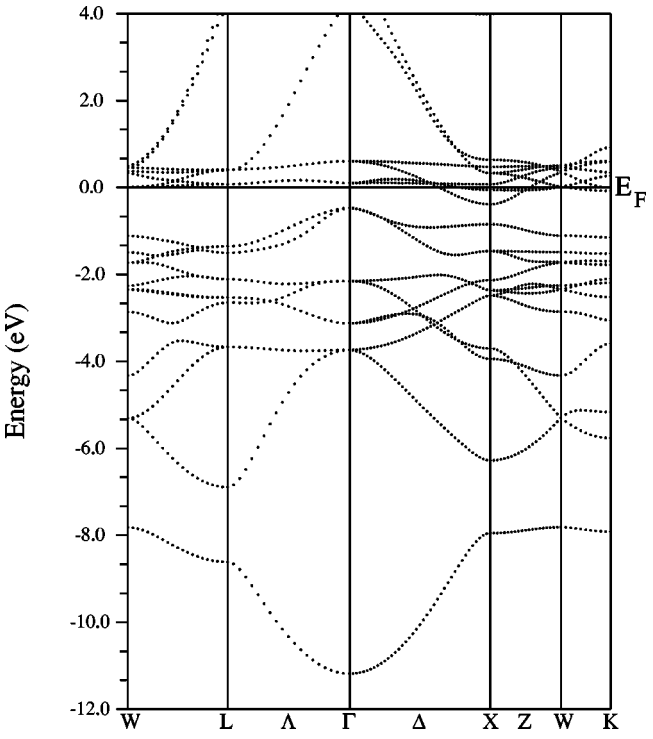

FIG. 4. The FLAPW band structure of ferromagnetic Co_2FeGa along the high-symmetry lines for the minority spin.

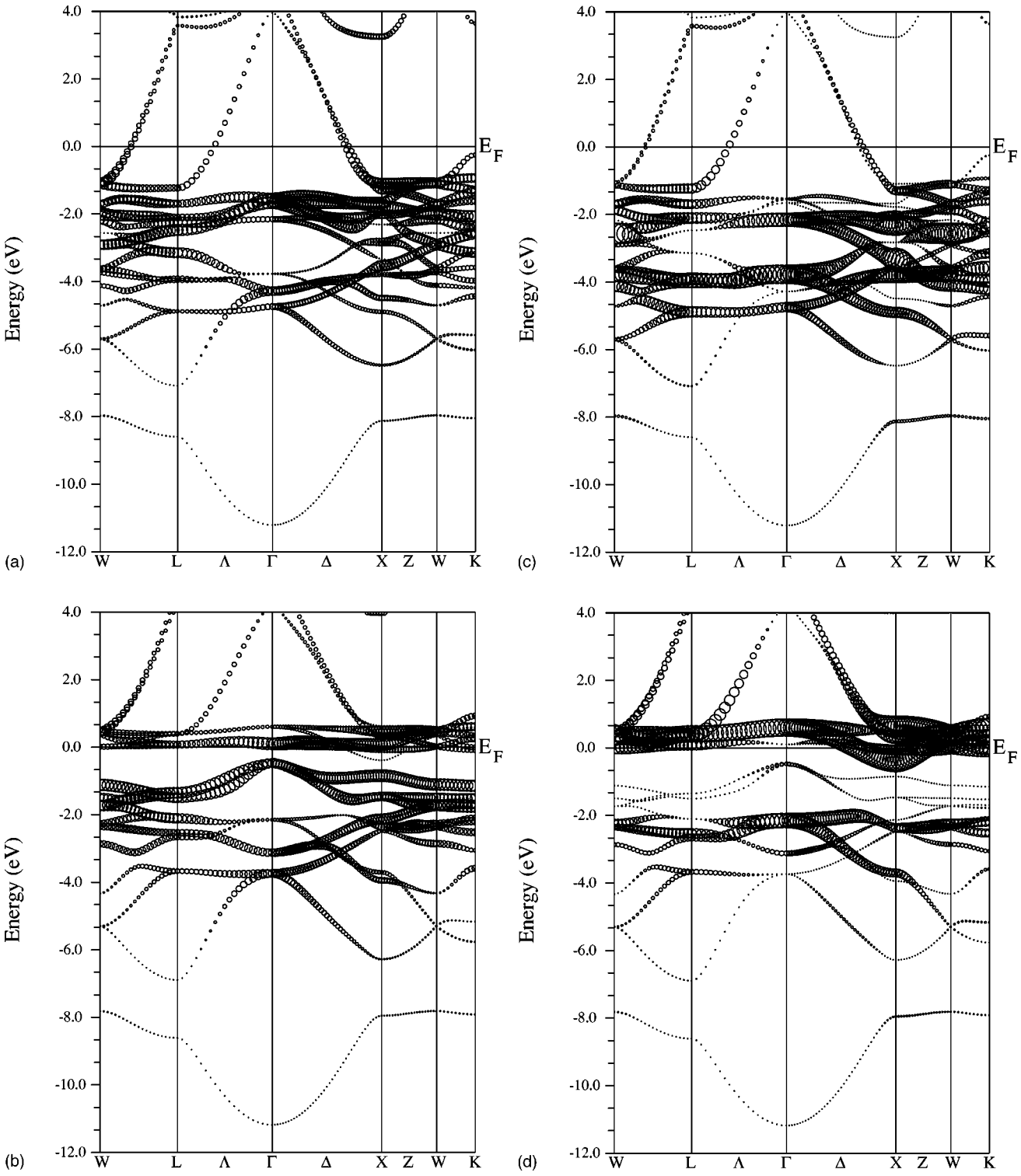

FIG. 5. The FLAPW-GGA band-character plots for Co_2FeGa: (a) Co-3*d* majority spin; (b) Co-3*d* minority spin; (c) Fe-3*d* majority spin; (d) Fe-3*d* minority spin. The symbol size here depicts the strength of the orbital character of the bands.

listed in Table I. The total magnetic moment in Co_2FeGa from the present calculation is found to be in good agreement with the corresponding experimental values. From Table I it is evident for the Co and Fe sites that there is a large preponderance of the e_g carriers. Our calculated values of the spin moment of the e_g and the t_{2g} sub-bands for the Co and the Fe sites are in excellent agreement with the recently reported neutron-diffraction measurements.[17]

Hyperfine parameters such as the hyperfine field (HFF) reveal important information regarding the interaction of a nucleus with the surrounding charge distribution. There are various techniques like Mössbauer spectroscopy, nuclear

TABLE I. Calculated site projected spin moment and total energy in Co_2FeGa. The *d*-orbital contribution is further broken down in e_g and t_{2g} component. Experimental values are shown in parentheses along with the temperatures at which the magnetic moments are measured and the available reported Curie temperature (T_C).

Co $3d$ moment (μ_B)			Fe $3d$ moment (μ_B)			Ga moment (μ_B)	Co_2FeGa molecule (μ_B)
d	d-e_g	d-t_{2g}	d	d-e_g	d-t_{2g}		5.03
						-0.07	(5.13,[a] $T=4.2$ K)
1.20	0.86	0.34	2.66	1.49	1.17		(4.72,[b] $T=223$ K,
	(0.72[b])	(0.34[b])		(1.46 [b])	(1.10[b])		$T_C>1100$ K)
Total energy (Ry/atom)						-10210.84	

[a]Buschow and van Engen (Ref. 16).
[b]Brown *et al.* (Ref. 17).

magnetic resonance, or perturbed angular correlation by which it can be measured. The dominant contribution to the hyperfine field results from the Fermi contact interaction and is given by the magnetization density at the nucleus. The three terms consisting of this dominant Fermi contact term, a dipolar term, and an orbital contribution constitutes the total hyperfine field (HFF). In this paper, we have considered only the contribution to the hyperfine field through the Fermi contact interaction, which within the scalar relativistic limit is obtained from the spin densities at the nuclear site,

$$H_c=\frac{8}{3}\pi\mu_B^2[\rho_\uparrow(0)-\rho_\downarrow(0)], \tag{3}$$

whereas within the fully relativistic scheme this spin density at the nucleus is substituted by its average over the Thomson radius $r_T=Ze^2/mc^2$.[42] For a better understanding of the origin of the hyperfine field we here have calculated the site projected valence electron contribution as well as the core contributions. Hyperfine fields at the constituent atoms of Co_2FeGa are listed in Table II, along with previously reported experimental values. It is important to note here that the absolute value of the valence and the core contribution of the hyperfine field at the Fe site are large and are of opposite signs. In Co_2FeGa where Fe has a large magnetic moment (about $2.66\mu_B$), the negative contributions to H_{val}(Co) from Fe moment is larger than the positive contribution from the Co moment itself. Hence the H_{val}(Co) value becomes negative. On the other hand the H_{val}(Fe) value is positive due to large magnetic moment of Fe. As discussed in the earlier studies[42] the core contribution to the HFF at the Fe site has a large negative value and can be qualitatively interpreted as follows. The majority-spin *s* electrons present in the core will be pulled into the region of the spin-polarized $3d$ shell, since the exchange interaction is attractive, whereas the minority-spin electrons will be repelled from the *d* shell. At the Fe nuclear position an excess of minority electrons, i.e., a negative polarization, is therefore created. Furthermore, since the local moment on the Ga site is negligible, the core contribution to the HFF at this site is small.

TABLE II. Calculated valence, core, and total contribution to the Fermi contact hyperfine field *H* in kG of the constituent atoms in Co_2FeGa. Experimental value is listed in column H_{exp}.

Compound		Valence (H_{val})	Core (H_{core})	Total (H_{tot})	Experiment (H_{exp})
	Co	-3.38	-147.80	-151.18	-182.0[a]
Co_2FeGa	Fe	110.23	$-3.22.65$	-212.42	
	Ga	-23.83	0.45	-23.37	

[a]Yoshimura *et al.* (Ref. 6).

V. TOTAL AND PARTIAL DENSITY OF STATES AND ELECTRON DENSITIES

The total and partial densities of states of Co_2FeGa was calculated utilizing the modified tetrahedron method of Blöchl *et al.*[43] The electronic state density (DOS) where ↑ represents the majority spin electrons and ↓ the minority spin

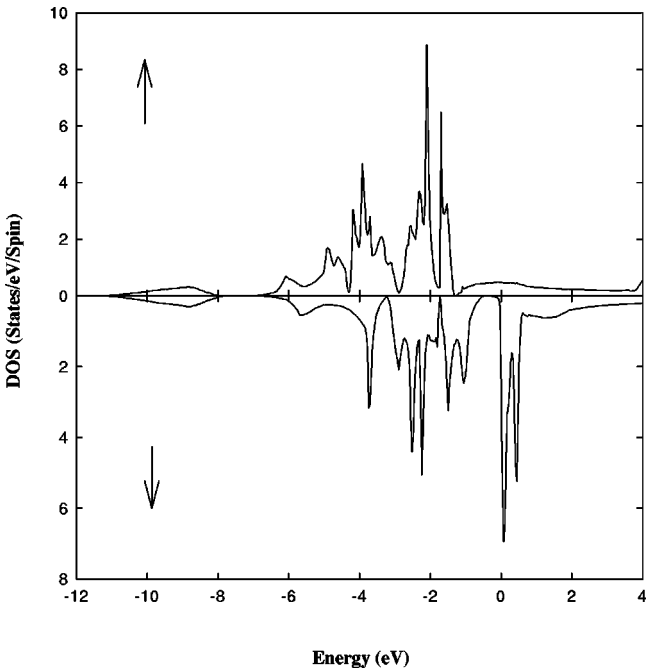

FIG. 6. Total majority (↑) and minority (↓) state densities per eV and unit cell for ferromagnetic Co_2FeGa.

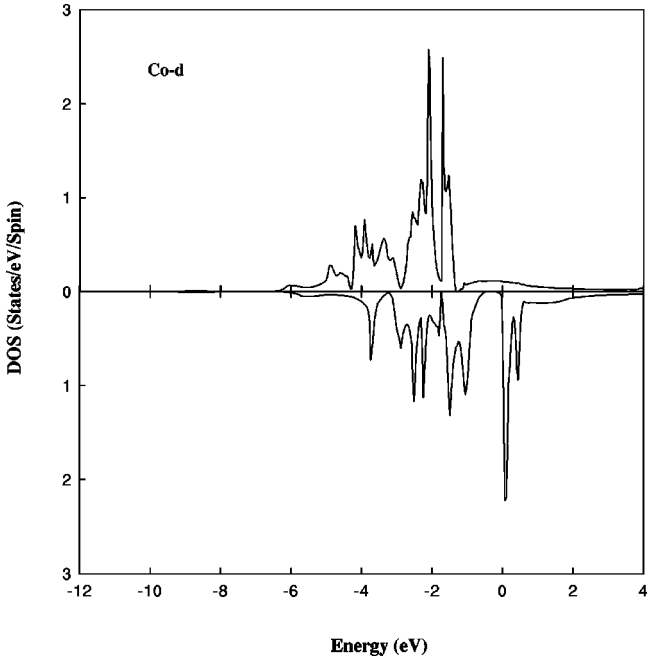

FIG. 7. Majority and minority spin *d*-electron state densities of Co plotted upward and downward for Co_2FeGa.

electrons is shown in Fig. 6. Decomposition of the total density of states which clarifies the origin of the peak structures, are presented in Figs. 7 and 8, respectively, showing the majority-spin and minority-spin *d* densities of states of Co and Fe. In Fig. 6 the region between -11 and -8 eV in the valence band shows the contribution from the Ga $4s$ states with small contributions from Co and Fe $4s$ states, while the rest of the valence bands of Co_2FeGa are mainly derived from the $3d$ electrons of Co and Fe. A close examination of

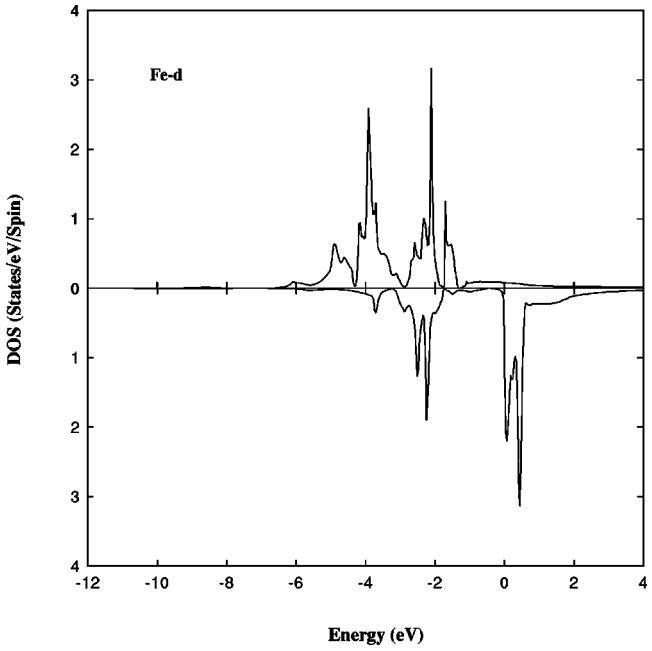

FIG. 8. Majority and minority spin *d*-electron state densities of Fe plotted upward and downward for Co_2FeGa.

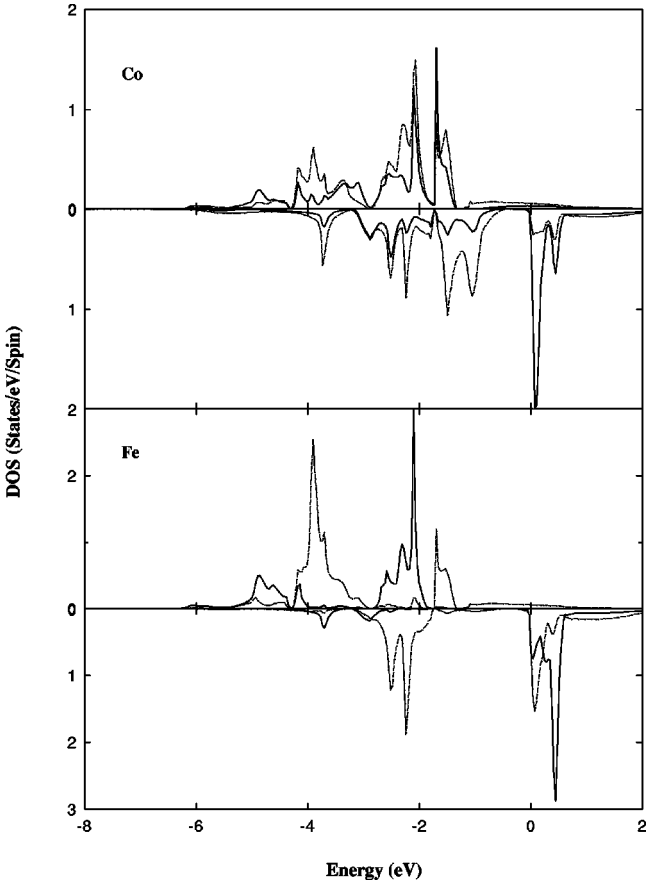

FIG. 9. Atom and symmetry projected density of states of Co_2FeGa, with majority plotted upward and minority plotted downward. e_g and t_{2g} symmetries are solid and dashed lines, respectively.

Figs. 7 and 8 reveals that for the majority spin the Co-*d* and Fe-*d* are mainly confined in the region between -6 and -1 eV, whereas for the minority spin in the conduction band (about 1 eV above the Fermi level) the Co-*d* states hybridize with the Fe-*d* states. The atom and symmetry projected densities of states (PDOS) of Co and Fe shown in Fig. 9, clarify the character of the bands. At the Co site, for the spin-up band in the valence band there is almost equal contributions from e_g and t_{2g} electrons. While for the minority spin, in the valence band the Co t_{2g} states are more dominating than the Co e_g states. For Fe the majority e_g band is nearly full and has negligible DOS at E_F, the higher DOS at E_F being in the t_{2g} band. However, there does not seem to be high enough DOS in the minority-spin e_g band below E_F. The present theory shows that the Co_2FeGa Heusler alloy cannot be classified as a half metallic ferromagnet.

In order to understand the electronic states of Co_2FeGa, we constructed the valence-electron density maps in the [110] plane. A detailed calculation of charge densities within FLAPW formulation was given by Blaha and Schwarz.[44] Figure 10 shows the plot of electron density corresponding to the valence band. The spin density $(\rho_\uparrow - \rho_\downarrow)$ map on the Co_2FeGa [110] plane is shown in Fig. 11. The large peaks on the three-dimensional graph coincide with the locations of the magnetic ions of Co and Fe. Thus it is evident from the

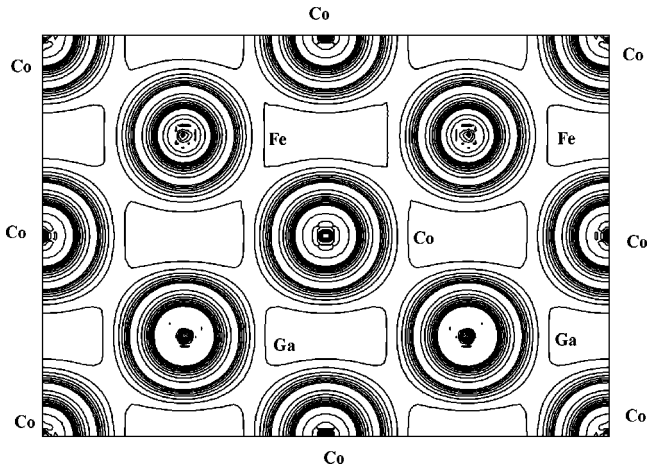

FIG. 10. FLAPW-GGA valence electron density in the [110] plane in units of 0.01 $e/\text{Å}^3$; logarithmic scale; contour lines differ by a factor of $\sqrt{2}$.

figure that magnetization results from both the Co and the Fe atoms. Furthermore the magnitude of the spin density is observed to be highest at the Fe site whereas around gallium (Ga), it is extremely small (Table I). As pointed out in the previous section, this magnetization at the Co and Fe site is mainly e_g in character.

VI. MAGNETIC COMPTON PROFILES

The experimental magnetic Compton profiles are shown in Fig. 12, together with those calculated by the FLAPW-GGA method, the latter after convolution with the experimental resolution. The experimental profiles are normalized to the 300-K magnetization of $5.10\mu_B$. The agreement is generally good but for $0<p<1$ a.u. the calculated values utilizing the FLAPW-GGA scheme overestimates the experimental values in all the three directions. The magnetic Compton profiles can be separated into the relative contributions from different atomic sites, by utilizing the Compton profiles for electrons in free atom[45] as a basis function to fit the magnetic line shape. Initially, to one, it might seem inappropriate to use a free atom basis, but successful results have been reported in the case of number of rare-earth and actinide ferromagnets.[46–48] This is mainly because the free-atom momentum densities must result in a good description of the momentum distribution away from the low-momentum region due to the following energy considerations. The kinetic energy of a system is determined either by the second moment of the Compton profile $[p_z^2 J(p_z)]$, or of the parent momentum density $[p^2 n(p)]$, and hence from the viral theorem, the total energy. Hence in this expression for the energy the high momentum density is progressively

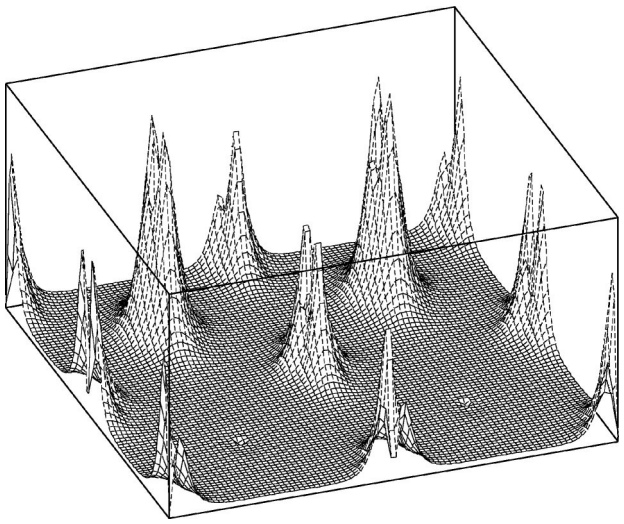

FIG. 11. FLAPW-GGA three-dimensional-plot of the spin density $(\rho_\uparrow - \rho_\downarrow)$ of Co_2FeGa in the [110] plane; linear scale, in units of $e/\text{Å}^3$.

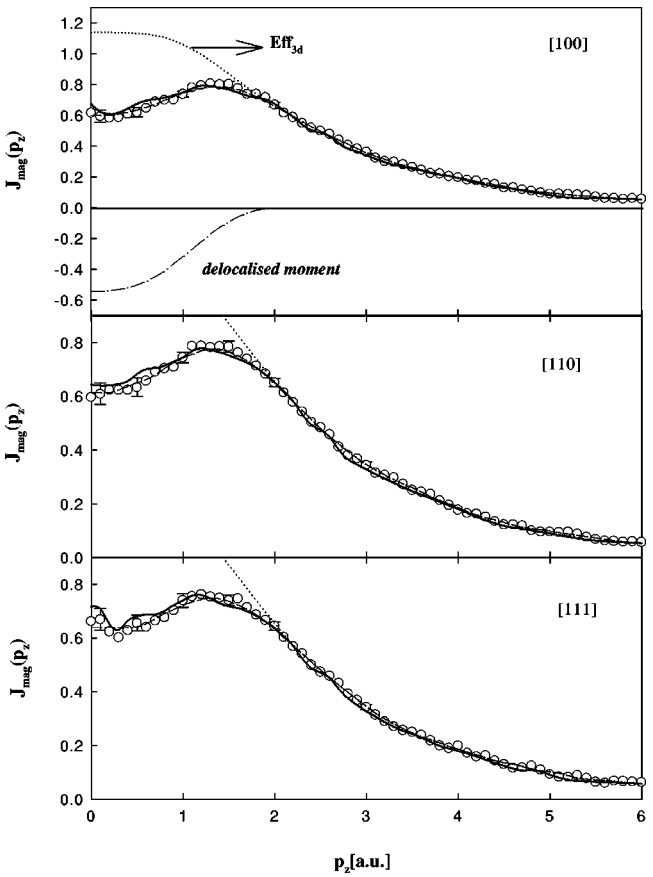

FIG. 12. The experimental and theoretical directional magnetic Compton profiles of Co_2FeGa normalized to $5.10\mu_B$. The open circles show the experimental data averaged over the low- and high-energy sides of the profile. The statistical errors at low momenta are shown by the error bars; at high momentum these errors are smaller than the diameter of the circles. The solid line represent our FLAPW-GGA calculated results convoluted with the experimental resolution of 0.66 a.u. Decomposition of the experimental data into the effective-$3d$ (Eff_{3d}) free-atom and free-electron Compton profiles are shown by dotted and dot-dashed curves, respectively (the latter curve has been shown only for the [100] direction) and were convoluted with the experimental resolution of 0.66 a.u. The areas under the effective $3d$ free-atom and free-electron profiles are $5.70\mu_B$ and $0.60\mu_B$, respectively. The dashed line represents the sums of the effective $3d$ (Eff_{3d}) and free-electron profiles and show the overall quality of the fits to the experimental data.

weighted by p^2. Moreover, the cohesive energies, proportional to the difference between these moments obtained for the solid and the free atom, constitute a small fraction of the total energy. So, keeping the p^2 weighting in mind, this difference can only derive from significant differences between the free-atom's and the solid's Compton profiles for the low-momentum behavior. At the high momenta the density distribution, and hence the Compton profiles, must be accurately free-atom like. Here for Co_2FeGa, the $3d$ free atom Compton profiles of Co and Fe are almost similar at the experimental resolution and separation of the two components are difficult. But as pointed out in the earlier section and also in Table I, the calculated $3d$ moments at the Co and the Fe sites are in good agreement with the recently reported neutron data.[17] Keeping this in mind, we obtained a weighted effective-$3d$ (Eff_{3d}) profile as

$$\mathrm{Eff}_{3d}=\frac{2\times \mathrm{Co}_{3d}}{5.03}\ \mathrm{FreeCo}_{3d}+\frac{\mathrm{Fe}_{3d}}{5.03}\ \mathrm{FreeFe}_{3d}, \qquad (4)$$

where FreeCo_{3d} and FreeFe_{3d} represents the $3d$ free-atom Compton profile of Co and Fe atom taken from Biggs *et al.*,[45] while $5.03\mu_B$ represents the calculated spin moment per unit formula and the whole profile was renormalized by the experimental magnetic moment of $5.10\,\mu_B$. The Co_{3d} ($1.20\mu_B$) and Fe_{3d} ($2.66\mu_B$) represents the theoretically calculated $3d$-moments of Co and Fe in Co_2FeGa, and are shown in Table I. It is important to note here that in finding the effective-$3d$ profile the presence of the two atoms of Co in Co_2FeGa has been taken into consideration by multiplying the first term of Eq. (4) by a factor 2. The magnetic Compton profiles of Co_2FeGa was then fitted by this resultant effective $3d$ free-atom profiles and a parabola, which is the profile appropriate to a free-electron, to describe the delocalized components, and are shown in Fig. 12. The average effective $3d$ moment was found to be $5.70\mu_B$, which leads to an average value of diffuse moment of $-0.60\mu_B$.

Referring to Fig. 12 it is clear that both the experiment and theory verifies the existence of a central dip at $p_z=0$, where the observed dip is slightly more than the calculated FLAPW-GGA values. This central dip at $p_z=0$ a.u. clearly indicates that the diffuse moment is opposed to the Fe-$3d$ and Co-$3d$ moments. This negative moment deduced from three directional measurements has an average value of $0.60\mu_B$. This contradicts the neutron data,[17] where a positive polarization was reported. Regarding this difference in observation in the neutron data and the MCP results, a probable reason may be that the neutron experiments does not measure directly the itinerant electron contribution, it is estimated from the saturation magnetization measurements and the diffraction data. While on the other hand MCP measurements can measure the itinerant electron contribution directly. In the case of a $3d$ shell of Fe and Co the polarization of diffuse (itinerant) electrons as a result of p-d hybridization with Ga electrons might result in either parallel or antiparallel spin alignments. The experiment shows unequivocally that the delocalized moment assigned to the diffuse electrons is antiferromagnetically coupled to the $3d$ moment at the Fe and Co sites.

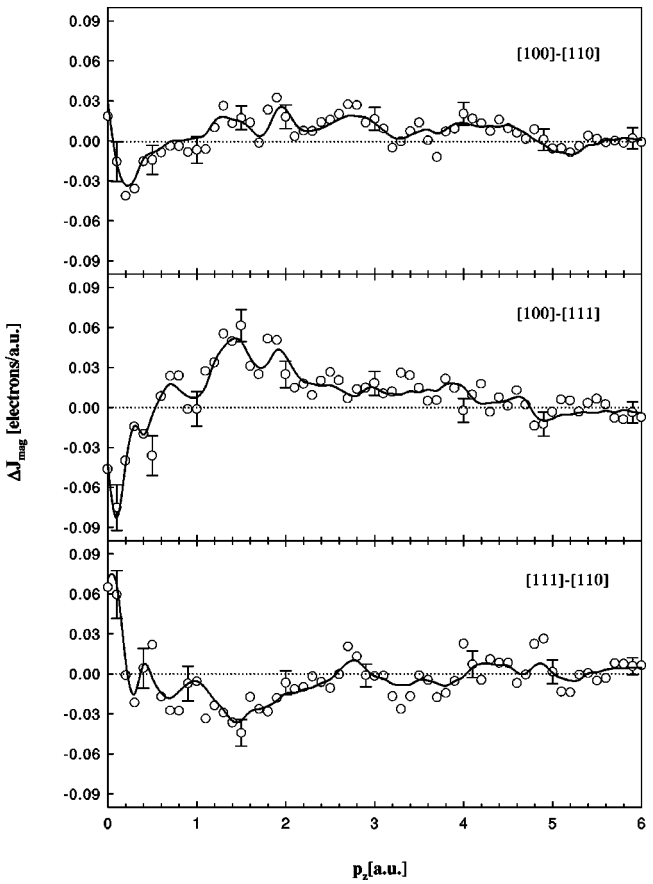

FIG. 13. Difference profiles reflecting the anisotropies in directional magnetic profiles of Co_2FeGa. The experimental and the theoretical differences are plotted by open circles and the solid lines, respectively. The theoretical data obtained from the FLAPW-GGA calculations was convoluted with the experimental resolution of 0.66 a.u.

According to the neutron data the anisotropy of the position space magnetization density for Heusler alloys, which is assumed to be the spin magnetization density, should be small; the same should also be true for the magnetic Compton profiles. As shown in Fig. 13, it is evident that the differences between the directional magnetic Compton profiles are significant, within the level of statistical errors. It is seen in Fig. 13 that there are some deviations from spericity at low momenta, which in general follow the indications of the theory (given by solid line). A close inspection of the individual profiles (Fig. 12) reveals that the differences between theory and experiment is more pronounced in the low-momentum region ($p_z<1$ a.u.) where our theoretical values overestimate the experimental results. But above 1 a.u. the theoretical results show very good agreement with the experimental values.

VII. SUMMARY AND CONCLUSIONS

The experiments and calculations presented in this work were undertaken to study the magnetic properties of Co_2FeGa, Heusler alloy. We have used the detailed theoretical calculations based on the FLAPW-GGA scheme. We

have also studied the trends in the spin moments, the spin density, and also hyperfine field and compared with the available reported experimental results wherever possible.

The hyperfine field was studied in order to examine the influence of the surrounding magnetic atoms on the magnetic properties of an atom. We have seen the magnetic properties of the Co atom in Co_2FeGa are easily influenced by the surrounding atom on account of the small magnetic moment (about $1.20\mu_B$ in Table I) on the Co site. At the Fe site the sign of the H_{core} has a high negative value while for H_{val}(Fe), there are two contributions; the positive contribution from its own moment and the negative one from the surrounding Co moments. The positive contribution becomes large because of the high moment at Fe site, hence summing up these contributions, the hyperfine field eventually becomes negative for Fe (Table II). It is also important to note that the hyperfine field of Co calculated within the FLAPW-GGA scheme is in good agreement with the previously reported experimental value of Yoshimura *et al.*[6] (Table II). The band-structure character plots in Figs. 5(a)–5(d) provide us a clear picture of the contributions of the different states of Co and Fe in the valence and the conduction bands for the majority and the minority spin, respectively. It is found that *d* bands of Fe approach and hybridize with the *d* bands of Co. From the band-structure analysis we found that for the majority-spin electrons the Fermi level cuts the spin-up bands, which is characteristic of a metallic band, along with a hole pocket centered at Γ, while for the minority-spin electrons the Fermi level lies at the bottom of the conduction band. Thus our band-structure calculation results suggest that Co_2FeGa, the compound in question, cannot be classified as a half metallic ferromagnet. Moving a step further we studied the atom and symmetry projected densities of states (PDOS) (Fig. 9), to clarify the character of the bands. In this context, it is important to note here that we studied individually the contribution of the Co and Fe-3*d* e_g and t_{2g} subbands. As seen from Table I the calculated d-e_g, t_{2g} contribution has been in excellent agreement with the recently reported neutron data, and confirms our results that the Co-3*d* and the Fe-3*d* moments are mainly d-e_g in character.

The Co-3*d* and Fe-3*d* contribution to the density of states extends to about 6 eV below the Fermi level. The contribution to the total density of states between -11.2 and -8 eV is from the Ga-4*s* orbital with small contributions from Co-4*s* and Fe-4*s* states. As summarized in Table I, the moment at the Fe site is much higher than at the Co site, which is also clearly evident from Fig. 11.

Finally, the magnetic Compton profiles from the FLAPW-GGA calculations are in good agreement with the experiment (Fig. 12). From our study it is evident that with $p_z < 1.0$ a.u. our theoretical results overestimates the experimental values, but above $p_z > 1.0$ a.u. our theoretical values are in excellent agreement with our measured data. The diffuse conduction electron contribution to the spin moment was about $-0.60\mu_B$ with an error of $\pm 0.04\mu_B$, in contradiction to the neutron data which reported a moment of $+0.43\mu_B$. On the other hand, the theoretical results for the 3*d* spin moment for Co and Fe ($1.20\mu_B$ and $2.66\mu_B$) along with their e_g and t_{2g} contributions are in excellent agreement with the neutron data.[17] Here we have used the present theoretical results for the individual moments of Co and Fe, to obtain the Eff_{3d} profile and hence the delocalized moment ($-0.60\mu_B$). As we have seen from the theoretical study the e_g moment dominates the Co and the Fe 3*d* moments, hence for the further study it will be interesting to observe the individual e_g contribution to the profile near $p_z = 0$. The experiment confirms that the majority and minority bands are anisotropic. The comparison with the experiment underlines the importance of performing calculations using a ferromagnetic ground state. From the experimental point of view, it will now be more interesting to study and investigate the specific features in these profiles which are not described well, i.e., the shape of the profiles at low momentum and the blurring of the umklapp features; utilizing the high-resolution measurements,[49–51] where $\Delta p \approx 0.15$ a.u. achievable with crystal spectrometers.

ACKNOWLEDGMENTS

We would like to thank Dr. O. Motohashi (JAERI), for the help in Laue photographs, and Professor N. Shiotani (Tokyo University of Fisheries) for providing us the sample. This experiment was done under the approval of SPring-8 Proposal No. 2000A0165-ND-np. We also acknowledge the support by the SPring-8 Joint Research Promotion Scheme under the auspices of Japan Science and Technology Agency.

*Corresponding author. FAX: +81-(0)7915-8-0830. Email address: ani12@spring8.or.jp

[1] T. Nakamichi and C. V. Stager, J. Magn. Magn. Mater. **31-34**, 85 (1983).
[2] P. J. Webster, J. Phys. Chem. Solids **32**, 1221 (1971).
[3] M. Kawakami, Y. Kasamatsu, and H. Ido, J. Magn. Magn. Mater. **70**, 265 (1987).
[4] M. Kawakami, Hyperfine Interact. **51**, 993 (1989).
[5] K. Le Dang, P. Veillet, and A. I. Campbell, J. Phys. F: Met. Phys. **8**, 1811 (1978).
[6] K. Yoshimura, A. Miyazaki, R. Vijayaraghavan, and Y. Nakamura, J. Magn. Magn. Mater. **53**, 189 (1985).
[7] Y. Noda and Y. Ishikawa, J. Phys. Soc. Jpn. **40**, 669 (1976).
[8] Y. Ishikawa, Physica B **91**, 130 (1977).
[9] K. Tajima, Y. Ishikawa, P. J. Webster, M. W. Stringfellow, D. Tocchetti, and K. R. A. Ziebeck, J. Phys. Soc. Jpn. **43**, 483 (1977).
[10] A. R. Williams, V. L. Moruzzi, C. D. Gelatt, Jr., and J. Kubler, J. Magn. Magn. Mater. **31-34**, 88 (1983).
[11] J. Kubler, A. R. Williams, and C. B. Sommer, Phys. Rev. B **28**, 1745 (1983).
[12] J. Kubler, Physica B **27**, 257 (1984).
[13] S. Fujii, S. Sugimura, S. Ishida, and S. Asano, J. Phys.: Condens. Matter **2**, 8583 (1990).
[14] S. Ishida, S. Akasawa, Y. Kubo, and J. Ishida, J. Phys. F: Met. Phys. **12**, 1111 (1982).
[15] J. Tobola, J. Pierre, S. Kaprzyk, R. V. Skolozdra, and M. A. Kouacou, J. Magn. Magn. Mater. **159**, 192 (1996).

[16] K. H. J. Buschow and P. G. Van Engen, J. Magn. Magn. Mater. **25**, 90 (1981).
[17] P. J. Brown, K. U. Neumann, P. J. Webster, and K. R. A. Ziebeck, J. Phys.: Condens. Matter **12**, 1827 (2000).
[18] J.-H. Park, E. Vescovo, H-J. Kim, C. Kwon, R. Ramesh, and T. Venkatesan, Nature (London) **392**, 794 (1998).
[19] W. E. Pickett, Phys. World **11**(7), 22 (1998).
[20] R. A. de Groot, F. M. Muller, P. G. Van Engen, and K. H. J. Buschow, Phys. Rev. Lett. **50**, 2024 (1983).
[21] S. Fujii, S. Ishida, and S. Asano, J. Phys. Soc. Jpn. **64**, 185 (1995).
[22] K. Schwarz, J. Phys. F: Met. Phys. **16**, L211 (1986).
[23] S. P. Lecois, P. B. Allen, and T. Saski, Phys. Rev. B **55**, 10 253 (1997).
[24] W. E. Pickett and D. J. Singh, J. Magn. Magn. Mater. **104-107**, 2072 (1992).
[25] I. K. Jassim, K-U. Neumann, D. Visser, P. J. Webster, and K. R. A. Ziebeck, J. Magn. Magn. Mater. **104-107**, 2072 (1992).
[26] P. Blaha, K. Schwarz, P. Sorantin, and S. B. Tricky, Comput. Phys. Commun. **59**, 399 (1990).
[27] D. Singh, Phys. Rev. B **43**, 6388 (1991).
[28] J. P. Perdew and Y. Wang, Phys. Rev. B **45**, 13 244 (1992).
[29] J. P. Perdew, S. Burke, and M. Ernwerhof, Phys. Rev. Lett. **77**, 3865 (1996).
[30] J. E. Jaffe, L. Zijing, and A. C. Hess, Phys. Rev. B **57**, 11 834 (1998).
[31] K. Kokko and M. P. Das, J. Phys.: Condens. Matter **10**, 1285 (1998); R. Zeller, M. Asato, T. Hoshino, J. Zabloudil, P. Weinberger, and P. H. Dederichs, Philos. Mag. B **78**, 417 (1998).
[32] A. Delin, L. Fast, O. Eriksson, and B. Johansson, J. Alloys Compd. **275-277**, 472 (1998).
[33] J. K. Dewhurst, J. E. Lowther, and L. T. Madzwara, Phys. Rev. B **55**, 11 003 (1997).
[34] A. Deb and Y. Sakurai, J. Phys.: Condens. Matter **12**, 2997 (2000).
[35] P. Blöchl, O. Jepsen, and O. K. Andersen, Phys. Rev. B **49**, 16 223 (1994).
[36] M. J. Cooper, Rep. Prog. Phys. **218**, 415 (1985).
[37] S. W. Lovesey, J. Phys.: Condens. Matter **8**, L353 (1996).
[38] N. Sakai, J. Appl. Crystallogr. **29**, 81 (1996).
[39] N. Sakai and K. Ono, Phys. Rev. Lett. **37**, 351 (1976).
[40] M. J. Cooper, D. Laundy, D. A. Cardwell, D. N. Timms, R. S. Holt, and G. Clark, Phys. Rev. B **34**, 5984 (1986).
[41] N. Sakai, H. Ohkubo, and Y. Namura, J. Synchrotron Radiat. **5**, 937 (1998).
[42] S. Blügel, H. Akai, R. Zeller, and P. H. Dedrichs, Phys. Rev. B **35**, 3271 (1987); A. J. Freeman and R. E. Watson, in *Magnetism*, edited by G. T. Rado and H. Shul (Academic, New York, 1965) Vol. IIA.
[43] P. E. Blöchl, O. Jepsen, and O. K. Andersen, Phys. Rev. B **49**, 16 223 (1994).
[44] P. Blaha and K. Schwarz, Int. J. Quantum Chem. **23**, 1535 (1983).
[45] F. Biggs, L. B. Mendelsohn, and J. B. Mann, At. Data Nucl. Data Tables **16**, 201 (1975).
[46] E. Zukowski, S. P. Collins, M. J. Cooper, D. N. Timms, F. Itoh, H. Sakurai, H. Kawata, Y. Tanaka, and A. Malinowski, J. Phys.: Condens. Matter **5**, 4077 (1993).
[47] M. J. Cooper, P. K. Lawson, M. A. G. Dixon, E. Zukowski, D. N. Timms, F. Itoh, H. Sakurai, H. Kawata, Y. Tanaka, and M. Ito, Phys. Rev. B **54**, 4068 (1996).
[48] P. K. Lawson, M. J. Cooper, M. A. G. Dixon, D. N. Timms, E. Zukowski, F. Itoh, and H. Sakurai, Phys. Rev. B **56**, 3239 (1997).
[49] Y. Sakurai, Y. Tanaka, A. Bansil, S. Kaprzyk, A. T. Stewart, Y. Nagashima, T. Hyodo, S. Nanao, H. Kawata, and N. Shiotani, Phys. Rev. Lett. **74**, 2252 (1995).
[50] S. Kaprzyk, Acta Phys. Pol. A **91**, 135 (1997).
[51] W. Schülke, G. Stutz, F. Wohlert, and A. Kaprolat, Phys. Rev. B **54**, 14 381 (1996).